Scientific Research Publishing

Open Journal of Civil Engineering, 2023, 13, 637-663
https://www.scirp.org/journal/ojce
ISSN Online: 2164-3172
ISSN Print: 2164-3164

Investigation on the Fire Resistance of Cellular Steel Beam with Sinusoidal Openings

Michee Sagali Mutentu[1], Bikoumou Gambat Maximino Horacio[2], Yinghua Yang[1]

[1]School of Civil Engineering, Xi'an University of Architecture and Technology, Xi'an, China
[2]School of Civil Engineering, Chang'an University, Xi'an, China
Email: michesagali@gmail.com, yhyang@xauat.edu.cn, bikoumouhoracio389@gmail.com

How to cite this paper: Mutentu, M.S., Horacio, B.G.M. and Yang, Y.H. (2023) Investigation on the Fire Resistance of Cellular Steel Beam with Sinusoidal Openings. *Open Journal of Civil Engineering*, **13**, 637-663.
https://doi.org/10.4236/ojce.2023.134043

Received: October 24, 2023
Accepted: December 4, 2023
Published: December 7, 2023

Abstract

This paper investigated the fire resistance of CSBs with various parameters under high temperature rise due to fire using finite element software ABAQUS. The mechanical parameters of CSBs are analyzed, including load-bearing capacity and the temperature distribution during the heating process. Through structural analysis simulation of the entire heating process, the structural response of the CSBs is divided into five stages: elastic stage, elastic-plastic stage, self-balancing stage, catenary stage and ultimate destruction stage. The results indicate that the opening diameter-to-height ratio, opening spacing- to-height ratio and load ratio significantly affect the structural responses of CSBs in fire, followed by opening shape as secondary effects. In all the numerical analyzes, CSBs are analyzed with a uniformly distributed load and having simply supported boundary conditions.

Keywords

Fire Resistance, Thermal and Structural Analysis, Cellular Steel Beam, Transient Temperature Effect

1. Introduction

Cellular steel beams (CSB) are getting more and more attention in the civil engineering community and are commonly used for long spans and heavily loaded floor system. They are generally built from hot rolled sections with oxy-cutting of the parent profile. Then the two parts of the parent profile are separated, positioned and finally welded so as to get the cellular beam. Thus, with the same weight, the cellular beam can reach 1.5 times the height of the parent profile. The use of CSB over the solid steel beam results in the enhancement of the bending stiffness. Shapes of the cellular beam can be made customize into vari-

ous looks of circular shape, octagonal shape, rectangular shape, hexagonal shape and sinusoidal shape. Among these, cellular beam with sinusoidal openings (Angelina beam) is more attractive with their fillet corner web holes with regard to architecture and engineering. Sinusoidal curves are designed for restraining concentration of stress. Moreover, cellular beams are also more convenient in terms of passing service pipes, wires and ventilating ducts through perforations (Chung 2002) [1]. Thus, the use of CSB results in more efficiency, good architectural appearance, long and stable spans without requiring any excess amount of steel material. **Figure 1** shows cellular beams used in parking structures.

However, introducing holes in the web can cause different modes of failure in CSB. The behaviour of CSB is very complex at ambient temperature and their responses under fire conditions are more complex so it is necessary to use finite element simulations to analyze their behaviour. There has been significant research work done on investigating the complex behaviour of cellular beams at ambient and elevated temperature. Lawson [2] presented a design method for simply-supported composite beams with rectangular openings in the web at ambient temperature. The design method is based on plastic analysis of the cross-sections, considering the moment transfer by Vierendeel action across openings. Chung *et al.* [3] have investigated the Vierendeel mechanism in steel beams with circular web openings based on analytical and numerical studies. Liu and Chung [4] have carried out a non-linear finite element analysis (FEA) investigation on steel beams with various shapes and sizes of web openings. Details of this design method are fully presented in a complementary paper [5]. Bailey [6] has investigated the temperatures experienced by the web-posts on cellular beams by carrying out preliminary indicative fire tests on unprotected and protected cellular and solid-web steel beams. Bitar *et al.* [7] proposed a model for web post resistance based on experimental studies and numerical investigations which covers symmetrical and unsymmetrical sections. Nadjai *et al.* [8] [9] carried out full-scale fire tests and numerical studies at both ambient and elevated temperatures. Four specimens, comprising two different steel geometries and loading conditions were tested at elevated temperatures. Vassart *et al.* [10] have conducted an extensive parametric study based on the tests results of four full-scale fire tests that have been conducted on composite cellular beams with circular and elongated web openings [11]. They have developed an analytical model that can be used for the prediction of the critical temperature of cellular beams. A full scale fire test has been performed recently on a composite floor for analyzing the possibility of tensile membrane action to develop when the unprotected steel beams in the central part of the floor are made of cellular beams [12]. At present there are only design guides addressing steel beams with web openings at ambient temperature as mentioned in annexe "N" of EC3 [13] and no uniform design guidelines are available for elevated temperature. There is less research work available on the fire resistance performance of cellular beam with sinusoidal openings under fire.


Figure 1. Applications of cellular beam with sinusoidal openings.

The present study aims to investigate the fire resistance performance of cellular beam adopted sinusoidal openings under fire conditions. The present work is carried out numerically using a one-way coupled field finite element analysis (FEA) considering geometrical and material nonlinearity. Parametric studies are performed under a three-sided heating regime by ISO-834 fire. A series of numerically based thermo-mechanical analyzes were performed for CSBs prepared from parent section H250 × 125 × 6 × 9 having simply supported boundary conditions. Study parameters include opening diameter-to-height ratio, opening spacing-to-height ratio, load ratio and shape of the web opening. The evolutions of the axial force and the mid-span deflection at the critical sections of CSBs with the elevation of temperatures are also presented.

2. Finite Element Model and Verification

The parametric study considering the aforementioned factors was done by performing numerical simulation in ABAQUS. The finite element model was first developed and validated with numerical simulation results available for solid steel beam subjected to fire reported in literature by Cong *et al.*, 2005 [14]. The validation process covers both thermal and structural predictions for results of solid steel beam and having simply supported boundary conditions.

2.1. Model Validation

The finite element model can give accurate results on conditions that we use the proper element type, element size, material model, boundary conditions, load conditions and solution technique, etc. For the lack of test results on fire resistance performance of CSBs under fire situation, simulation results on the solid web steel beam carried out by Cong *et al.*, 2005 [14] were used to verify the applicability of the finite element model.

The beam dimensions used in the verification were H250 × 125 × 6 × 9 and the span length of the beam was 4.2 m. The simply supported steel beam was loaded by four concentrated forces applied at four locations which is equivalent to the uniformly distributed load of 10 kN/m, as shown in **Figure 2(a)**. Both supports and beam ends in 150 mm range were fire protected. The simply supported beam was heated by a horizontal furnace with oil burner as shown in

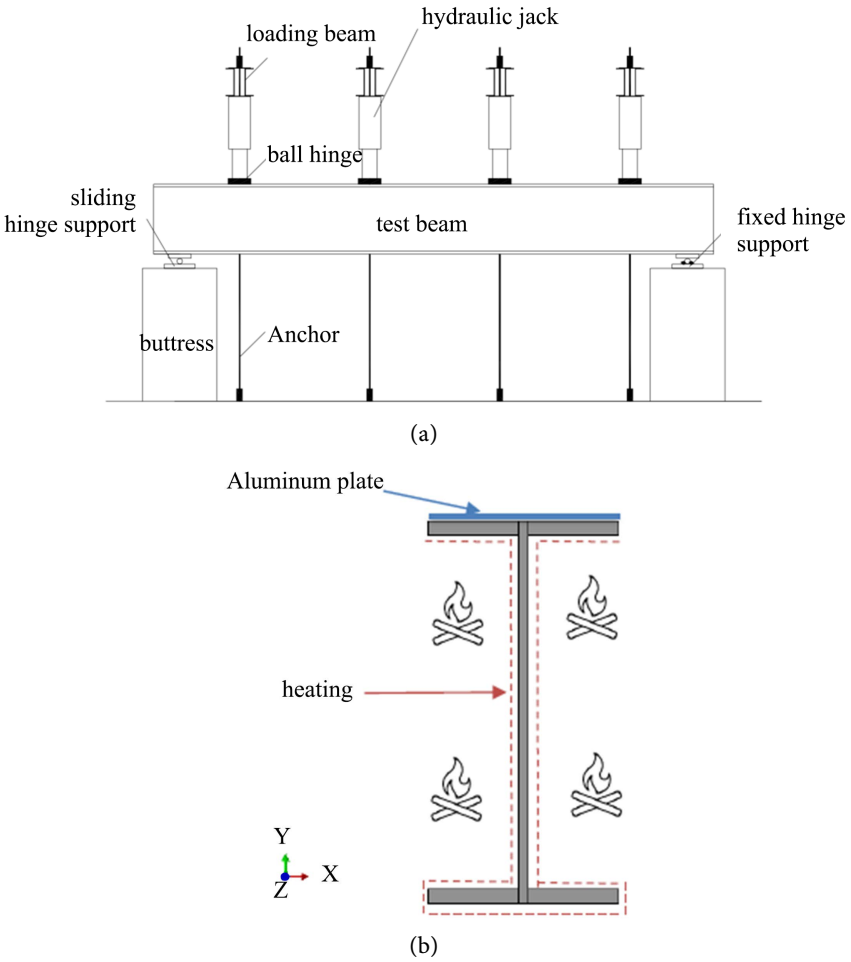

Figure 2. I-beam geometry and loading parameter along with surface exposed in fire. (a) Simply supported beam under four-point loading; (b) fire heating.

Figure 2(b). The top flange was covered by aluminium plate and exposed to air. The air temperature was considered as room temperature. All other sides were directly exposed to fire. The beam end adopts a relatively ideal hinge support form, one end is fixed hinge support, and the other end is sliding hinge support. The test beam adopts hot-rolled with steel properties Q235-B, the measured yield strength is 330 MPa, tensile strength is 415 MPa.

The validation process covers both thermal and structural predictions and having hinge-roller boundary conditions. **Figure 3(a)** compares the results of attained steel beam temperature from the present developed numerical model and that reported in Cong *et al.*, 2005 [14].

Figure 3(b) compares the results of the structural response of mid-span vertical displacement versus time from test results and that obtained from the developed finite element model. The pattern of temperature distribution and structural response obtained from the present developed model is consistent with that reported in Cong *et al.*, 2005 [14], which showed the applicability of the proposed finite element model for studying behaviors of steel beam in a fire.

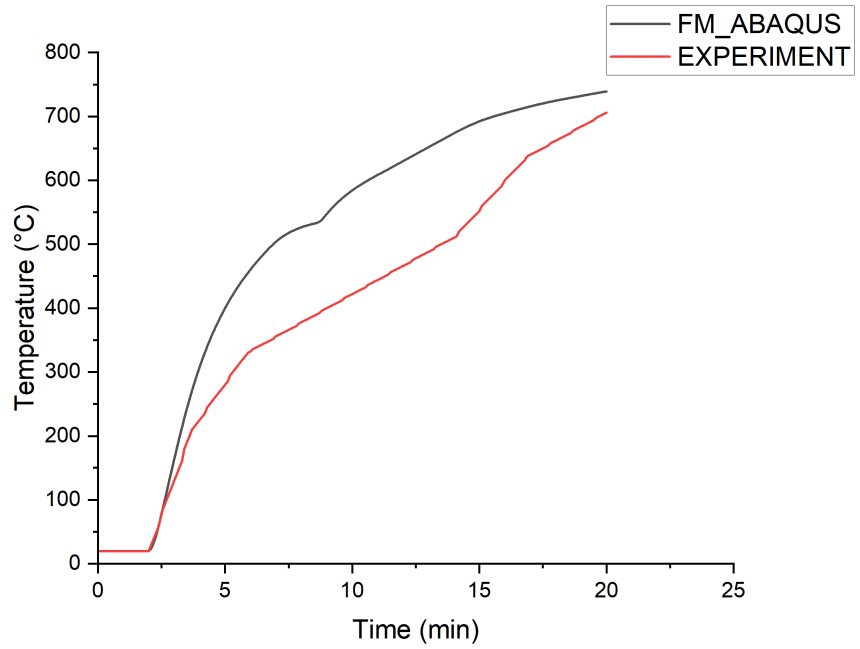

(a)

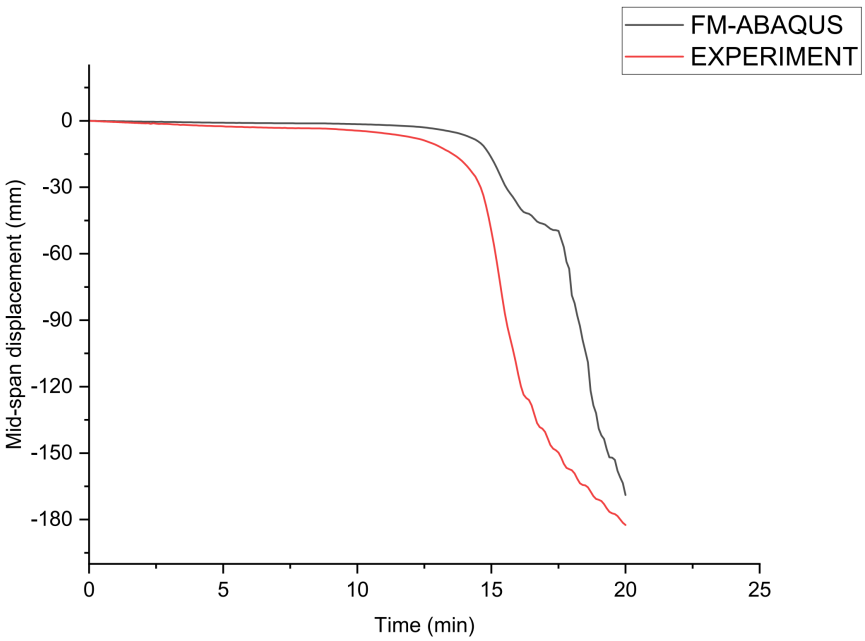

(b)

Figure 3. Comparison between FEA Abaqus and test results. (a) Time-Temperature distribution curve; (b) Mid-span deflection verse time.

2.2. Establishment of the Finite Element Model of CSBs

FE models were addressed in three steps:

1) Radiation and convection heat transfer analysis was performed separately to the CSBs, and the temperature was increased in accordance with the ISO-834 time-temperature curve;

2) General static analysis, in which the load was applied at room temperature and continues to the next step;

3) Quasi-static (VISCO) analysis was performed in order to combine previous steps, in which the predefined field (temperature) was used to import the temperature data results from step 1 to the CSBs.

The thermal and structural analysis model of restrained CSBs for simply supported boundary condition at the bottom flange was developed for carrying out further parametric analysis.

2.3. Thermal Analysis

The target of thermal analysis is to predict the temperature distribution in beam cross-section. FE models were simulated for 3D structure of I-beam using shell element. The thermal analysis includes transient heat transfer analysis with temperature-dependent thermal material properties, boundary convection and radiation. The thermal simulation requires the temperature-dependent thermal properties to be incorporated for analyzing the CSBs under fire conditions.

The equation for obtaining thermal material data for steel is discussed in this part. To reflect the thermal responses of CSBs more precisely, in this paper, the stress-strain relation, thermal conductivity, density, and specific heat capacity of steel were defined according to EC4 [15] as listed in **Table 1**.

During the thermal analysis process, thermal conductance, thermal convection and thermal radiation were all taken into account. The CSBs was heated from three sides by convection and radiation with the elevated gas temperature. The upper side of top flange beam was unexposed side and directly exposed to air of 20˚C. The lower side of top flange, bottom flange and beam web side were exposed to fire. In this case, temperature of the upper side top flange will only elevate due to thermal conduction. A graph figure for specific heat capacity and thermal conductivity, with steel temperature is illustrated in **Figure 4**.

Table 1. Thermal material properties of steel.

Materials	Calculations
Density ρ (kg/m^3)	7850
Thermal conductivity λs [W/mK]	$\begin{cases} 54-3.33\times10^{-2}T_S & 20\le T_S\le 800^{\circ}\text{C} \\ 27.3 & T_S\ge 800^{\circ}\text{C} \end{cases}$
Specific heat capacity Cs [J/kgK]	$\begin{cases} 425+7.73\times10^{-1}T_S-1.69\times10^{-3}T_S^2+2.22\times10^{-6}T_S^3 & 20\le T_S\le 600^{\circ}\text{C} \\ 666+\dfrac{13002}{738-T_S} & 600\le T_S\le 735^{\circ}\text{C} \\ 545+\dfrac{17820}{T_S-731} & 735\le T_S\le 900^{\circ}\text{C} \\ 650 & 900\le T_S\le 1200^{\circ}\text{C} \end{cases}$

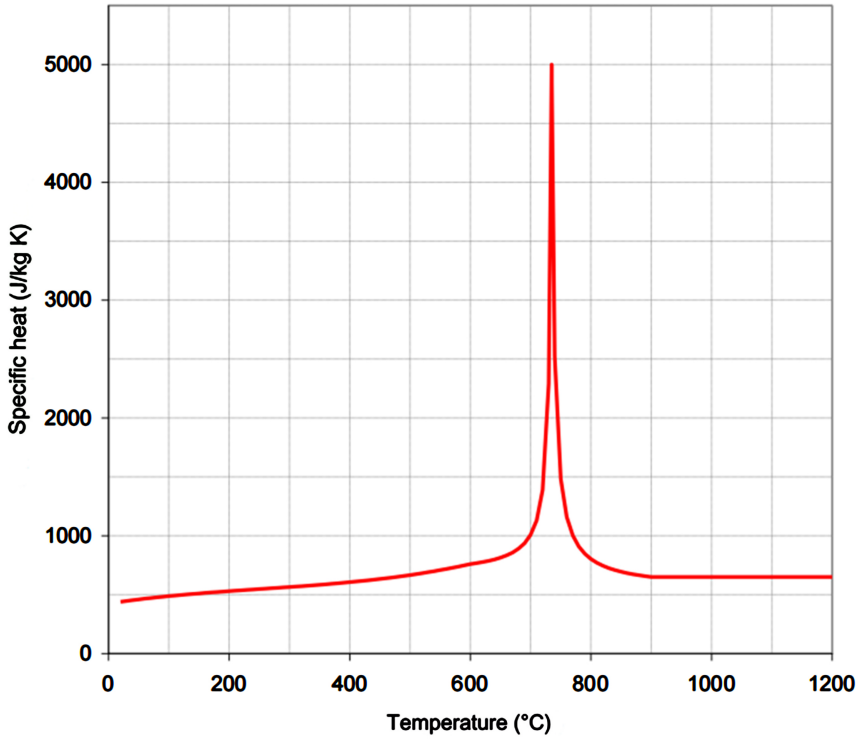

(a)

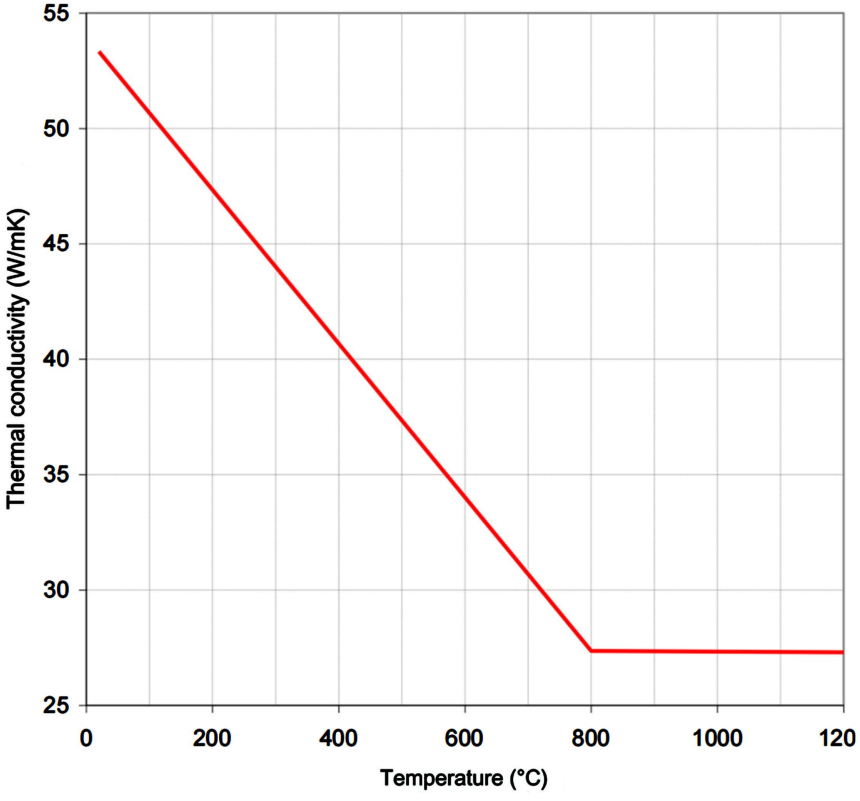

(b)

Figure 4. Specific heat and thermal conductivity of steel at elevated temperature. (a) Specific heat; (b) Thermal conductivity.

With the elevated gas temperature, the temperature of steel beam arises by radiative and convective heat transfer. The boundary convection set was defined in the 3D thermal model for convection heat transfer and boundary radiation set was defined for radiation heat transfer. The heat input due to convection between surfaces of steel beam and the hot gas is

$$q = \alpha_c \left(T_S - T_\infty \right) \tag{1}$$

where α_c is the convection coefficient (W/m^2·K). According to EC1 [16], the convection factor of 25 W/m^2·K was used in the exposed side, and 9 W/m^2·K was used in the unexposed side under ISO-834 standard fire for this thermal analysis. T_s is the surface temperature of steel beam (˚C), and T_∞ is the gas temperature (˚C).

The heat input due to the radiation is

$$q = \varepsilon \varphi \sigma \left[\left(T_S + 273 \right)^4 - \left(T_\infty + 273 \right)^4 \right] \tag{2}$$

where φ is configuration factor, taken as 1.0 in this analysis; σ is Stephan-Boltzmann constant (5.67 × 10^{-8} W/m^4·K^4); ε is the resultant emissivity coefficient, taken as 0.7 according to EC3 [17].

Figure 5 shows the temperature distribution contour in the beam section for 3D thermal model, the mapping of temperature distribution in structural analysis was very efficient using a 3D thermal model.

2.4. Structural Analysis

Structural analysis model predicts the structural response of structural member when mechanical loading and fire are present in the structure. This research used sequential thermal-stress analysis that requires two analyses in which heat transfer analysis is performed first to obtain the nodal temperature distribution, and then, a stress analysis is performed in which temperature is applied as external nodal loads to generate the thermal strain. Thermal expansion and temperature-dependent material properties are influenced by nodal temperature input. The structural analysis includes highly nonlinear analysis, including

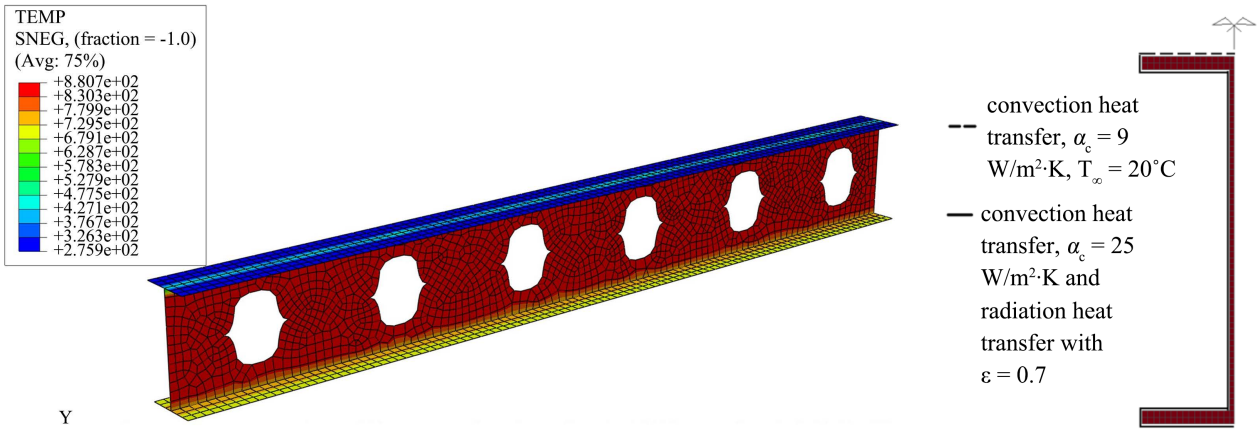

Figure 5. Thermal model results from 3D temperature analysis using shell element for CSBs.

nonlinear material, and deformation. The structural simulation requires the temperature-dependent mechanical properties to be incorporated for analyzing the CSBs under fire conditions. The mechanical materials used for structural analysis include: temperature-dependent isotropic elasticity, temperature-dependent coefficient of thermal expansion, temperature-dependent plasticity and density. All mechanical properties were defined according to EC3 [17] as listed in Table 2.

3. Nonlinear Analysis of CSBs under Fire

In this research study, thermal-stress analysis was performed using Abaqus/CAE [18]. In the process of simulating the fire resistance of CSBs, different connection methods will provide different constraints. Therefore, it is necessary to consider the mutual influence of components to simplify the model accurately and reasonably. As shown in Figure 6, vertical and lateral displacements at beam ends were constrained. Axial and rotational displacements were limited by setting the spring elements to simulate the constraints by columns. Because the top flange of CSBs was fixed with a floor slab, lateral displacement of top flange was restrained, considering shear studs were uniformly applied between CSBs and floor slab. Therefore, the finite element model is simplified as shown in the Figure 6. Where K_A represents the axial restraint stiffness of the steel beam, K_R represents the rotational restraint stiffness.

The geometric dimensions of CSBs were; H500 × 250 × 12 × 18, span length L = 4.2 m, opening spacing S = 700 mm, opening height a_o = 300 mm and load ratio of 0.5 corresponding to uniform distributed load. The FE analysis was carried out to obtain the structural response of CSBs at elevated temperatures. To simulate

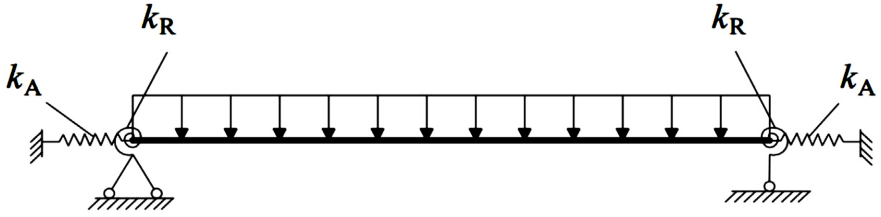

Figure 6. Model simplification.

Table 2. Mechanical material properties of steel.

Materials	Calculations
Density ρ (kg/m^3)	7850
Poisson's ratio υ	0.3
Thermal expansion coefficient αs	$\begin{cases} 0.8\times10^{-8}\left(T_S-20\right)+1.2\times10^{-5} & 20\le T_S\le 750^{\circ}\text{C} \\ 0 & 750\le T_S\le 860^{\circ}\text{C} \\ 2.0\times10^{-5} & 860\le T_S\le 1200^{\circ}\text{C} \end{cases}$
Plastic strain ε	0

simply supported beams, the hinge support for CSBs at left-end was simulated by restraining it against translations in X, Y and Z directions. The hinge support for CSBs on the right-end was simulated by restraining it against translations in X and Y directions. An overview of the numerical model including the reference system and the boundary conditions adopted can be seen in Figure 7.

The axial restraint of the CSBs was simulated through the spring element, spring 2, in ABAQUS. The steel beam was simply supported with both ends elastically restrained in the axial direction. The ends of the beam were constrained through the Multi-Point Constraint (MPC) in ABAQUS to assure that the ends section remains in plan under the loading and heating actions. The ends section can rotate around the MPC control point in the y-axis to simulate the pin support boundary conditions. The displacement of the ends section along the z-axis was the same to that of the MPC control point. The MPC control point is connected to a fixed point through the spring element, Spring 2, in the z direction to simulate the elastic axial restraint, as shown in Figure 8. The X and Y transitional degrees of the MPC control point were fixed. The three transitional

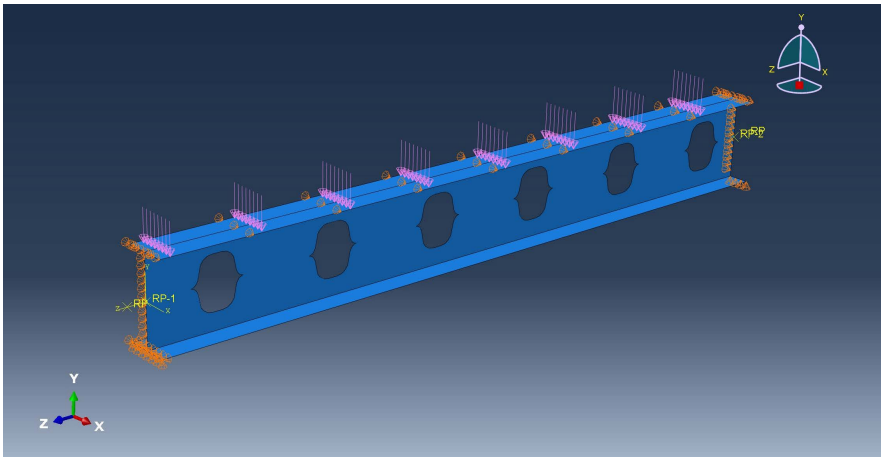

Figure 7. Loading and Boundary conditions of CSBs.

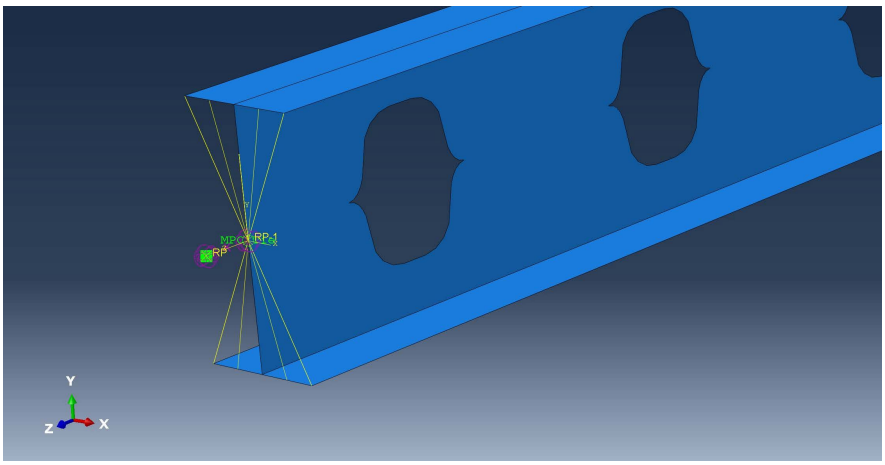

Figure 8. Boundary conditions of CSBs.

degrees of the MPC control point at the other end, X, Y and Z, were fixed. That is, the end section at right side was hinge supported that can rotate freely. A uniformly distributed load was applied at the top flange of the CSBs. The lateral displacement of the top flange was restrained in X direction to prevent the flexural torsional buckling of the beam.

The I-beam was modelled using S4R (a 4-node doubly curved thin or thick shell, reduced integration, hourglass control, finite membrane strains) shell element from Abaqus explicit element library. A mesh size of 40 mm was adopted for meshing the flanges as shown in Figure 9. Uniform mesh across the geometry was defined. Newton-Raphson method was used for nonlinear analysis.

The finite element simulation of the CSBs was carried out in three steps:

1) The uniformly distributed load corresponding to a given load ratio was applied in the first step to the top flange of CSBs for about 3 minutes (180 seconds) at its ambient temperature of 20˚C and kept constant in the fire loading step;

2) In the second step, the steel temperature was linearly elevated following the given distribution profile across the section, while the applied load was kept constant.

3) Finally, the nonlinear (material nonlinearity and geometry nonlinearity) analysis was carried out to obtain the total structural response of CSBs under elevated temperature.

After investigating the fire resistance performance of CSBs, it was found that the CSBs will go through 5 stages during the heating process: elastic stage (I), elastic-plastic stage (II), self-balancing stage (III), catenary stage (IV) and ultimate destruction stage (V). According to the stages of the CSBs, the simplified diagrams of the entire process of the CSBs under fire are shown in Figure 10.

The five nodes in Figure 10: A, B, C, D, and E are the ends of stages I, II, III, IV, and V respectively. At different stages, the mechanical response of the CSBs changes greatly. The above process can be better understood with the help of the finite element analysis process of CSBs. Figure 11 illustrates the heating process of above-mentioned CSBs.

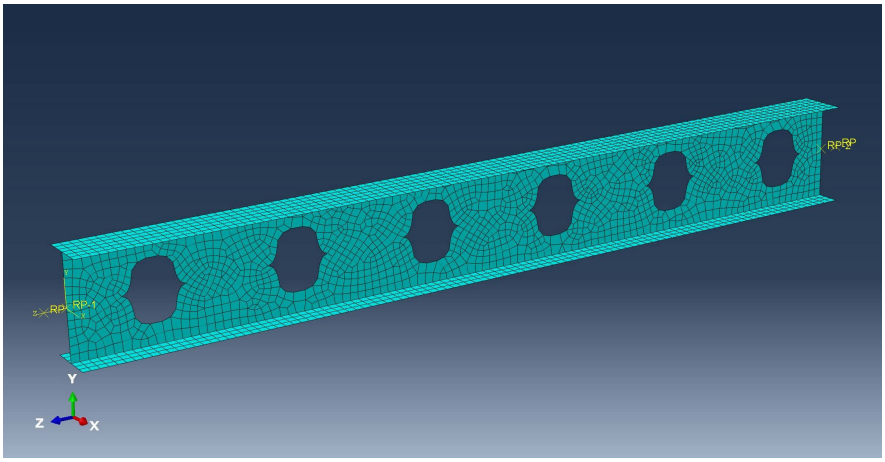

Figure 9. Quadrilateral-element meshing diagram of CSBs.

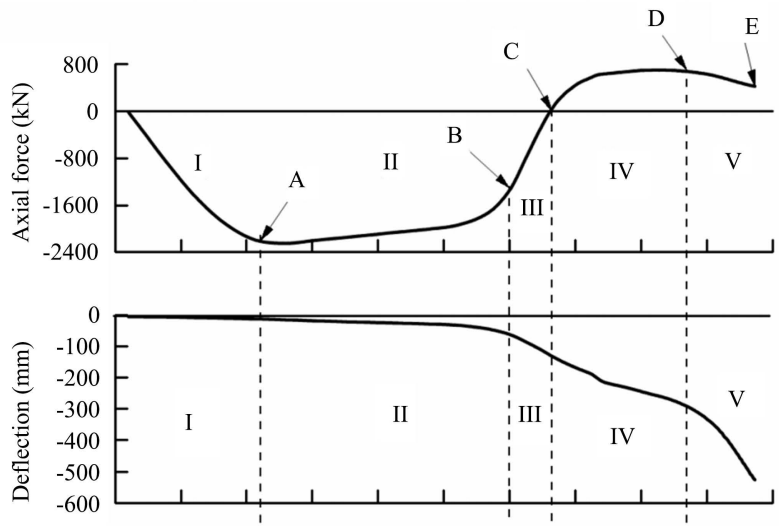

Figure 10. Brief diagram of the whole process of CSBs exposed to fire.

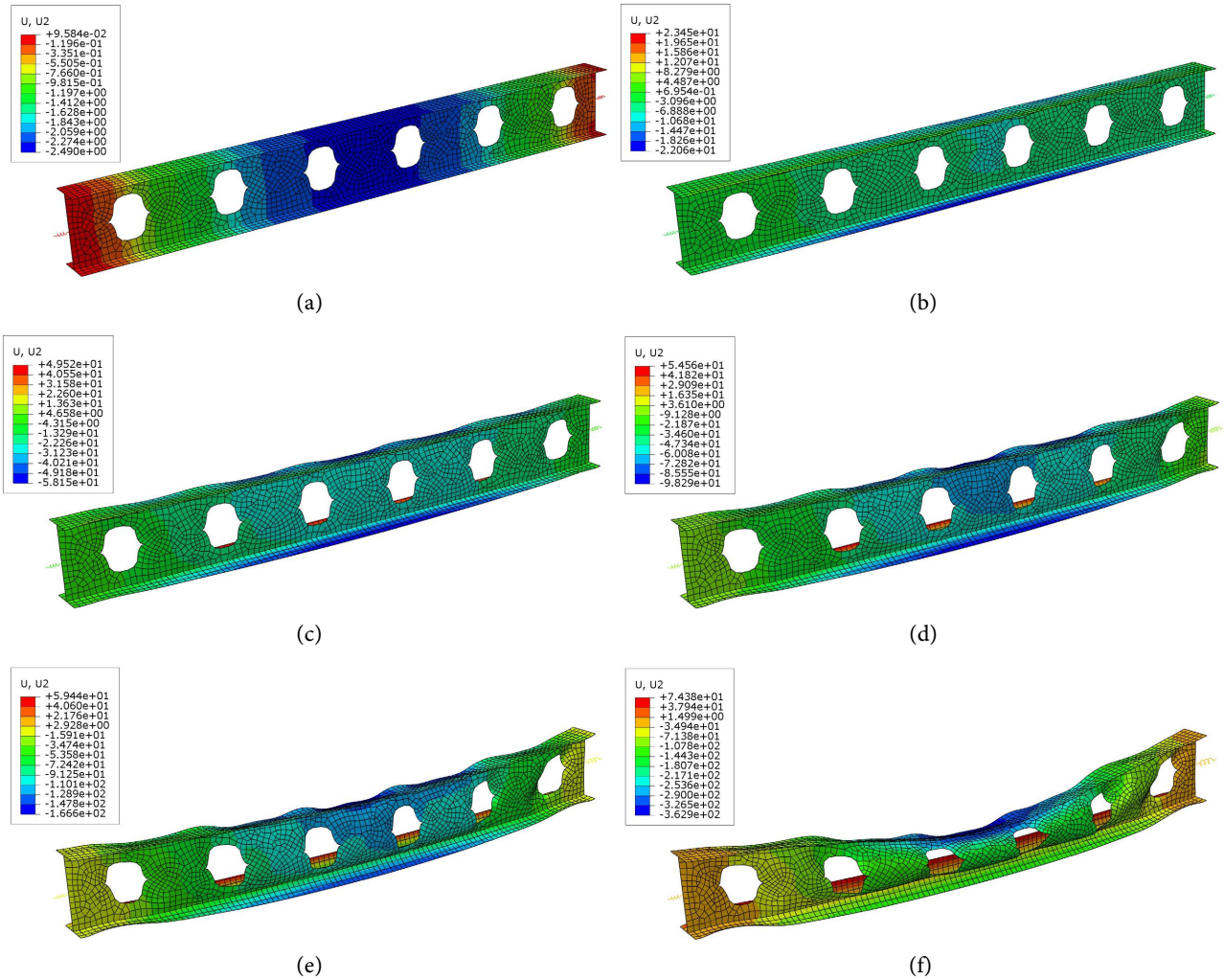

Figure 11. State of CSBs at various stage. (a) Ambient temperature (b) Stage I (elastic); (c) Stage II (elastic-plastic); (d) Stage III (self-balancing); (e) Stage IV (catenary action) (f) Stage V (ultimate destruction).

4. Parametric Study on the Structural Responses of CSBs in Fire

Multiple factors can influence the thermal and structural responses of CSBs at elevated temperatures, such as boundary conditions, geometric dimensioning, strength classes of structural steel, and load ratio. Therefore, four groups of CSBs were investigated; trying to quantify to what degree the multiple factors may affect structural responses of CSBs under fire. Dimensions of CSBs used in this section are illustrated in Figure 12.

Where S stands for spacing of openings, a_o is the height or diameter of openings, w is the length of the intermediate web post, ls is the length of sinusoidal part, r is the radius of fillet corner, tf is thickness of beam flange, tw is thickness of beam web, bf is the width of beam flange, and Ht is the overall depth of beam. The considered factors in this study were opening diameter-to-height ratio, opening spacing-to-height ratio, web opening shape and load ratio. In subsequent study, axial restraint stiffness ratio is indicated by α, rotational restraint stiffness ratio by β, load ratio by μ, structural yield strength of steel by f_y, opening spacing-to-height ratio by η and opening diameter-to-height ratio by γ.

4.1. Effect of Opening Diameter-to-Height Ratio γ

Opening diameter-to-height ratio γ is defined as the ratio of opening diameter and height of CSBs itself. Opening height is the most vital dimension, which has a great effect on the bearing capacity, saving amount of steel and aesthetic, etc. Its value directly affects the web utilization form of CSBs.

$$\gamma = \frac{a_o}{Ht} \tag{3}$$

The selected values of γ are 0.4, 0.6, 0.8 and 0.9 respectively. The dimension and design parameters of CSBs in this part are as follows: The beam section is H500 × 250 × 12 × 18, span length L = 4.2 m, axial restraint stiffness α = 1 and rotational restraint stiffness β = 1. The beam was loaded by a uniformly distributed load and having simply supported boundary conditions. The geometric parameters and dimensions of the CSBs are described in Figure 13 and Table 3.

The temperature change curves of the axial force and mid-span deflection are shown in Figure 14.

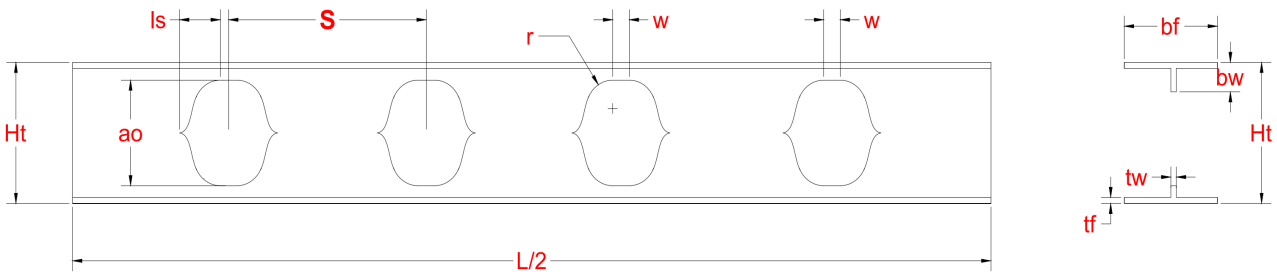

Figure 12. Dimensions of CSBs used in subsequent parameter study.

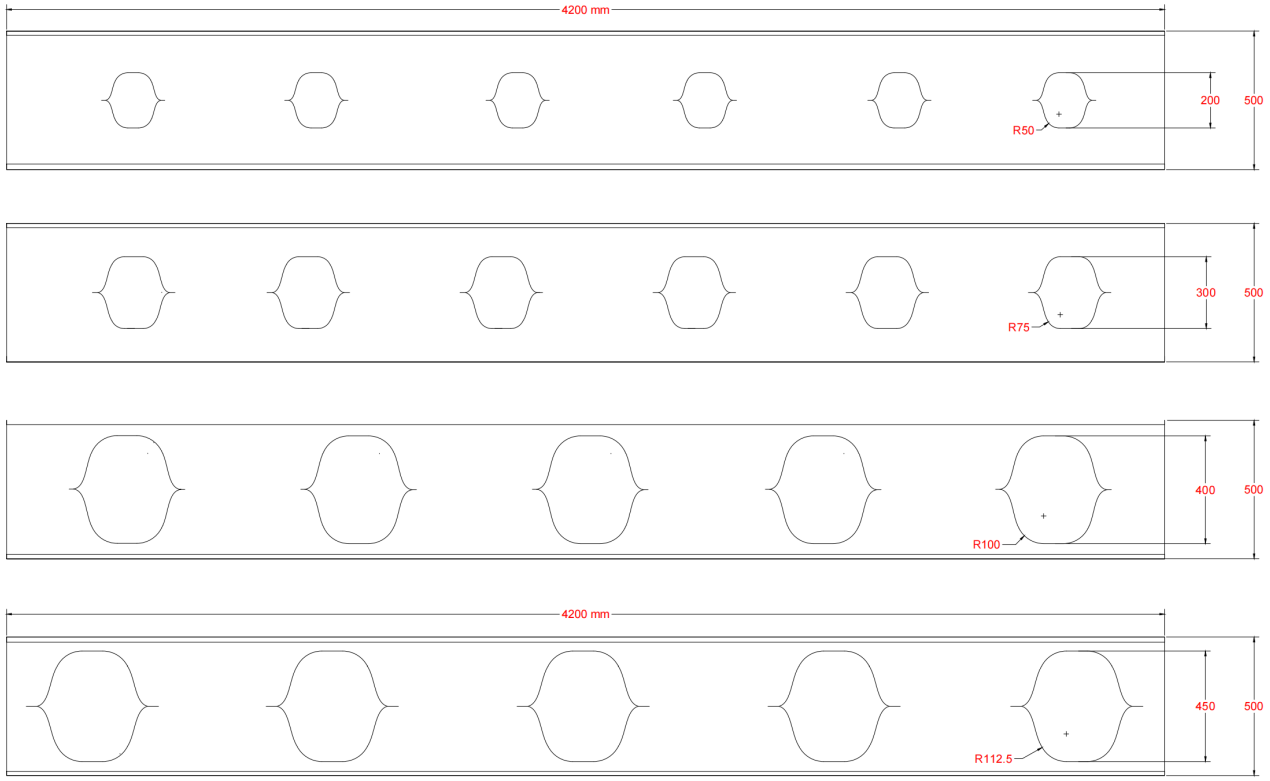

Figure 13. Geometric dimensions of CSBs with different openings height.

Table 3. Geometric parameters of CSBs with different opening diameter-to-height ratio.

Opening diameter-to-height ratio γ	0.4	0.6	0.8	0.9
Opening height (mm)	200	300	400	450
Opening spacing (mm)	700	700	700	700
Length of intermediate web-post (mm)	38.2	57.29	76.39	85.94
Number of opening holes	6	6	6	6
Load ratio	0.5	0.5	0.5	0.5
Fillet radius	50	75	100	112.5

The variation of γ affects the performance of CSBs much more than other parameters. It can be seen in **Figure 14**, as the parameter γ increases, there is a corresponding decrease in axial force due to the reduction in the equivalent of compressive web-post area. As γ reaches to 0.9, axial force and mid-span deflection declined earlier. However, catenary actions are delayed when γ exceeds 0.6, as large openings form around beam ends. Furthermore, the higher the value of opening diameter-to-height ratio γ, the smaller the equivalent compressive web-post area that can be achieved. As a result, the ultimate catenary action decreases. As shown in **Figure 14(b)**, in elastic-plastic stage, due to the reduction in the amount of steel used and the increase of opening diameter-to-height ratio

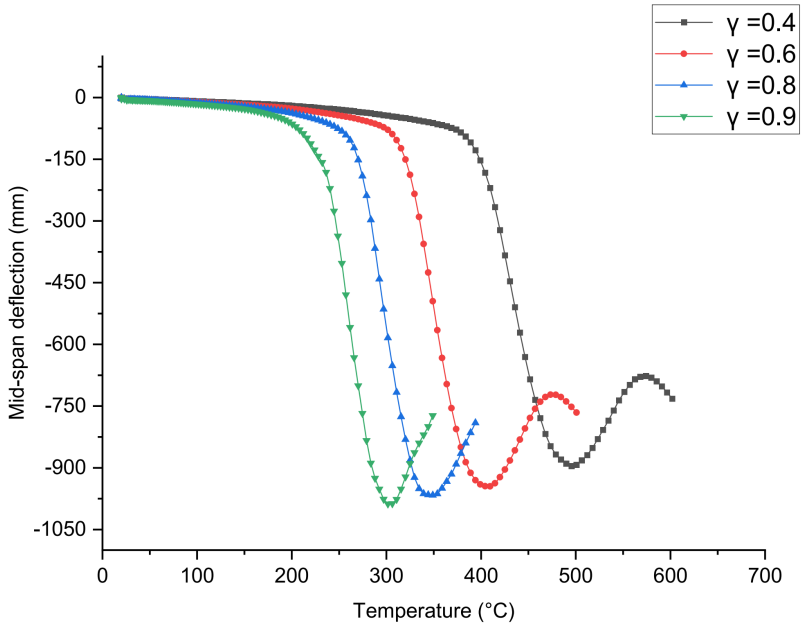

(a)

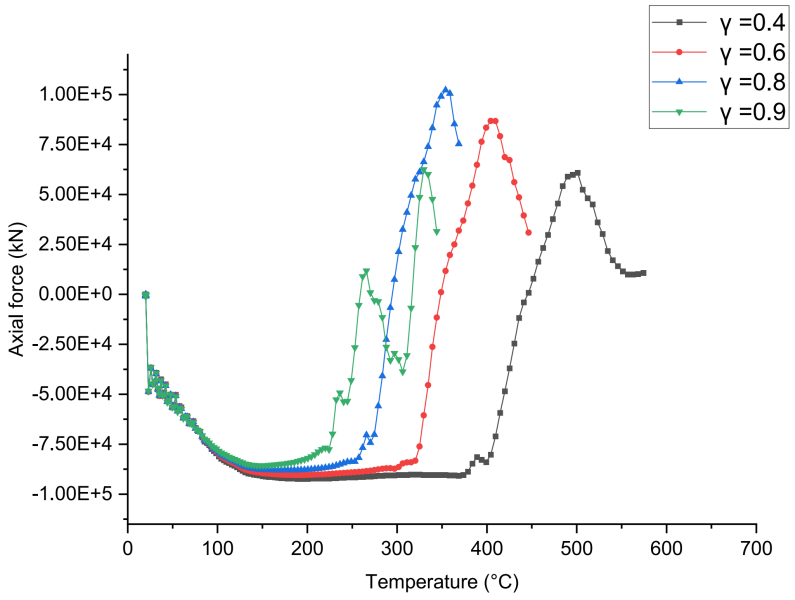

(b)

Figure 14. Effect of openings diameter-to-height ratio on structural responses of CSBs. (a) Mid-span deflection-temperature curve; (b) Axial force-temperature curve.

γ, the thermal expansion of steel decreases under heating. Therefore, as γ increases, the axial force on the steel decreases. Additionally, due to the decrease in stiffness, the maximum axial force increases significantly when γ falls within the range of 0.8 - 0.9 and the bearing capacity of CSBs will also decrease.

As seen in **Figure 15**, for CSBs whose γ is less than 0.8, bending failure is an essential form. When $\gamma \geq 0.8$, beam end section at first opening is the most critical section, which arouse shear deformation. Therefore, the reasonable interval

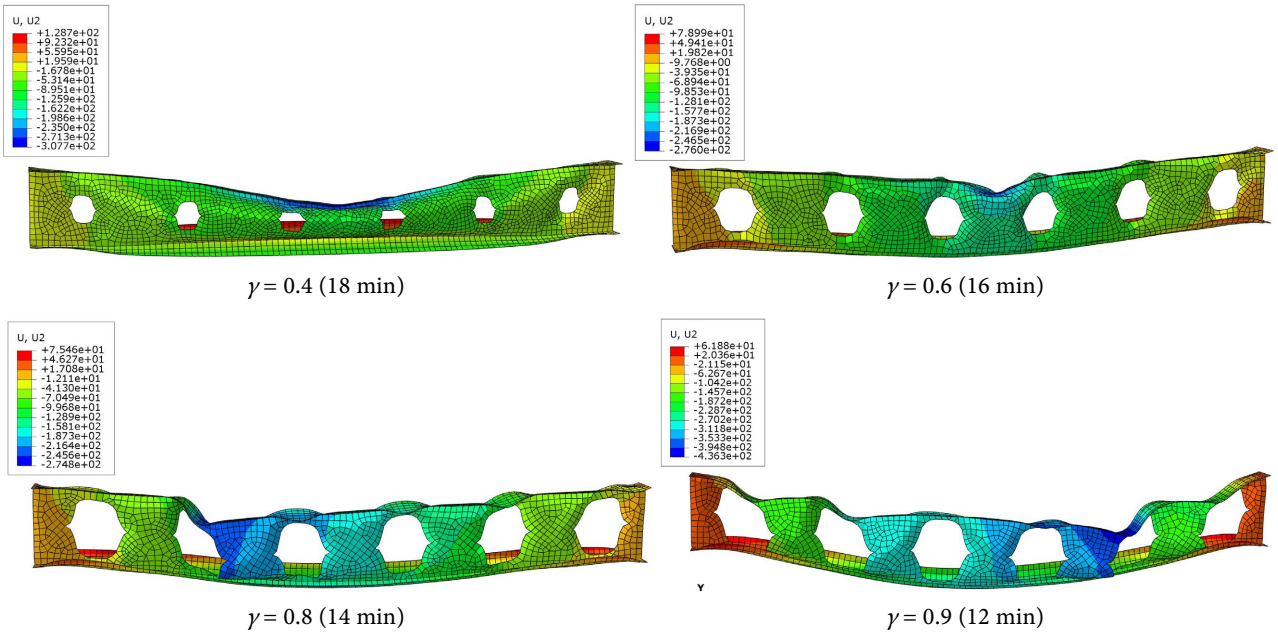

$\gamma = 0.4$ (18 min) $\gamma = 0.6$ (16 min)

$\gamma = 0.8$ (14 min) $\gamma = 0.9$ (12 min)

Figure 15. Failure mode of CSBs with varied opening diameter-to-height ratio.

of opening diameter-to-height ratio γ is within 0.4 - 0.6. The varying of γ has a huge impact on the fire resistance perfomance of cellular beam with sinusoidal openings. Thus, γ should be regarded as a critical factor in this study.

4.2. Effect of Opening Spacing-to-Height Ratio η

Opening spacing-to-height ratio η is defined as the ratio of opening spacing and the total height of CSBs.

$$\eta = \frac{S}{Ht} \tag{4}$$

The value of η should be chosen within proper interval. The selected values of η in this part are 1, 1.2, 1.4 and 1.6 respectively. The dimension and design parameters of CSBs in this part are as follows: The beam section is H500 × 250 × 12 × 18, span length $L = 4.2$ m, axial restraint stiffness $\alpha = 1$ and rotational restraint stiffness $\beta = 1$. The beam was loaded by a uniformly distributed load and having simply supported boundary conditions. The geometric and dimensions parameters of CSBs are described in **Figure 16** and **Table 4**.

The temperature change curves of the axial force and mid-span deflection are shown in **Figure 17**.

Figure 17(a), it is expected that higher opening spacing-to-height ratio will bring about earlier descending of mid-span displacement whereas the displacement is impacted by variations of η in a large degree. Analyzing the axial force in **Figure 17(b)**, in elastic stage, the axial force curves corresponding to different η basically coincide, in this stage η has little effect on axial force. From elastic-plastic stage the axial force will increase as η increases. The reason is analyzed: the wider is the web-post, the overall bearing capacity of the structure increases

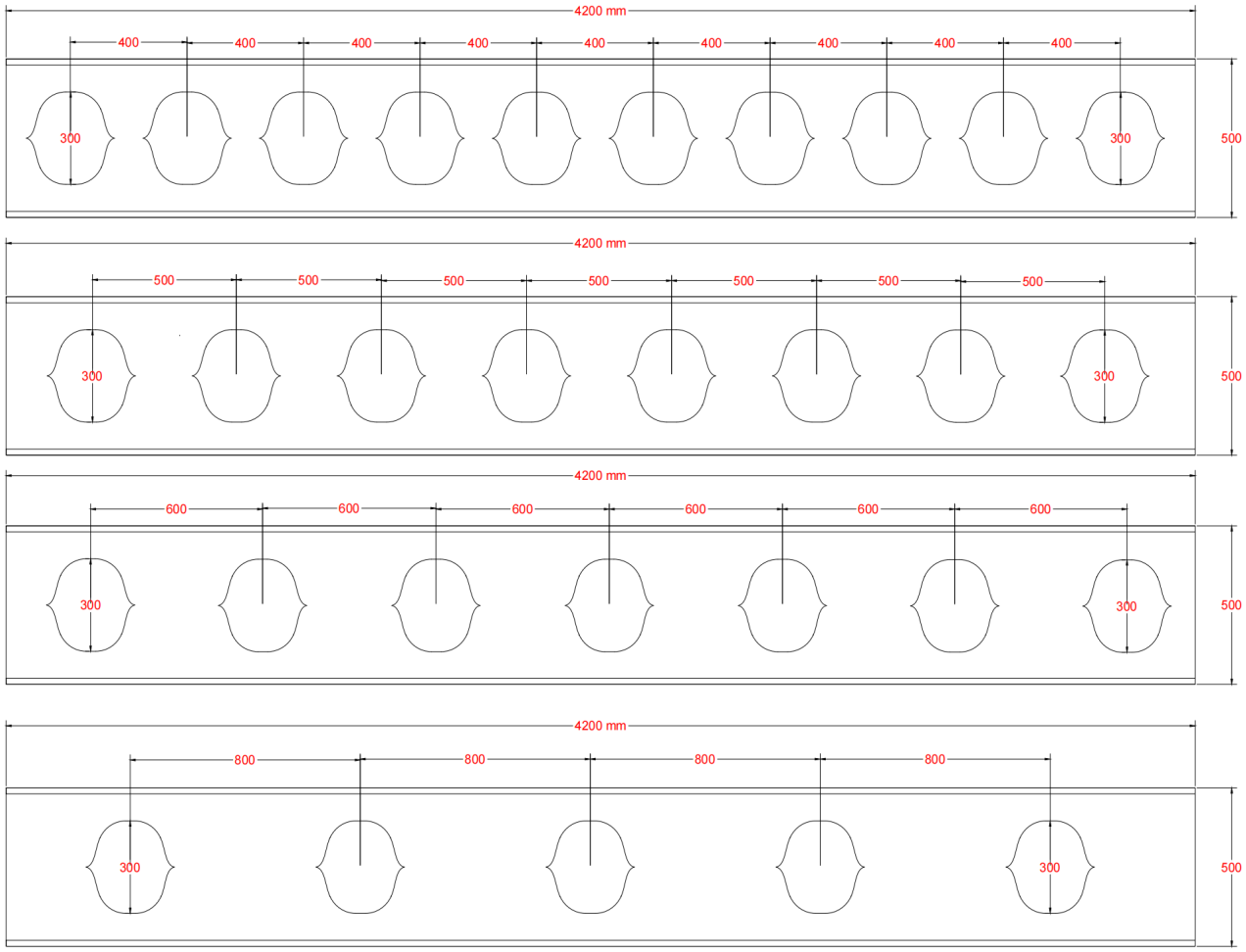

Figure 16. Geometric dimensions of CSBs with different openings spacing.

Table 4. Geometric parameters of CSBs with different opening spacing-to-height ratio.

Opening spacing-to-height ratio η	1	1.2	1.4	1.6
Opening height (mm)	300	300	300	300
Opening spacing (mm)	500	600	700	800
Number of opening holes	8	7	6	5
Fillet radius	75	75	75	75
Load ratio	0.5	0.5	0.5	0.5

slightly. However, after entering catenary action stage, shear capacity increases while η raises from 1.2 to 1.4, the maximum axial tension is reached at η = 1.2. At this time, when η increases to a certain value, the positive impact caused by the widening of the web-post cannot resist the negative impact caused by stress concentration around opening holes, and shear deformation is prone to occur, affecting the load-bearing capacity of the CSBs.

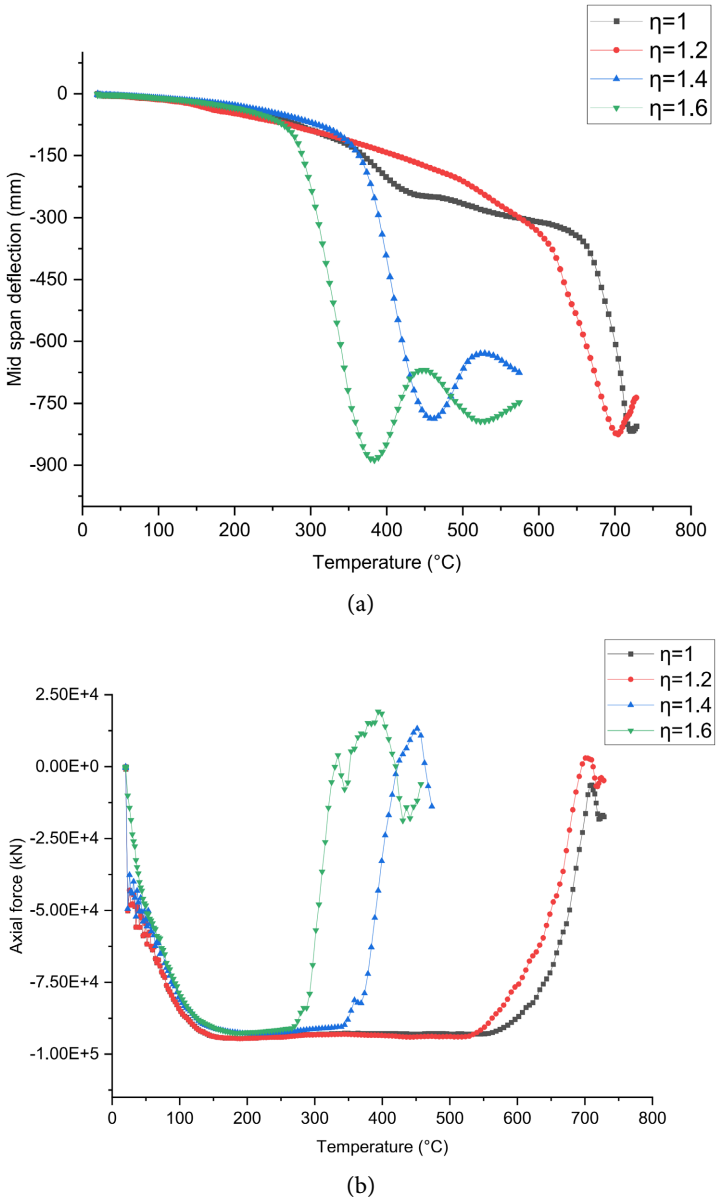

Figure 17. Effect of openings spacing-to-height ratio on structural responses of CSBs. (a) Mid-span deflection-temperature curve; (b) Axial force-temperature curve.

With the increase of web-post spacing between openings, the bearing capacity is greatly affected. When the beam opening spacing η is too small, the web-post is narrow and torsional buckling is prone to occur. When η is too big (1.4 - 1.6), the mid-span deflection occurs earlier and the beam can bear the load within a short period of time, which is particularly dangerous for structural safety when fire occurs. Through the failure mode and failure time shown in **Figure 18**, fatal buckling can be observed at both web post and lower flange when $\eta \leq 1.2$ due to insufficient width of web-post, as well as the buckling at both web around first opening from beam-end and lower flange. As a result, the reasonable interval of η is 1 - 1.4.

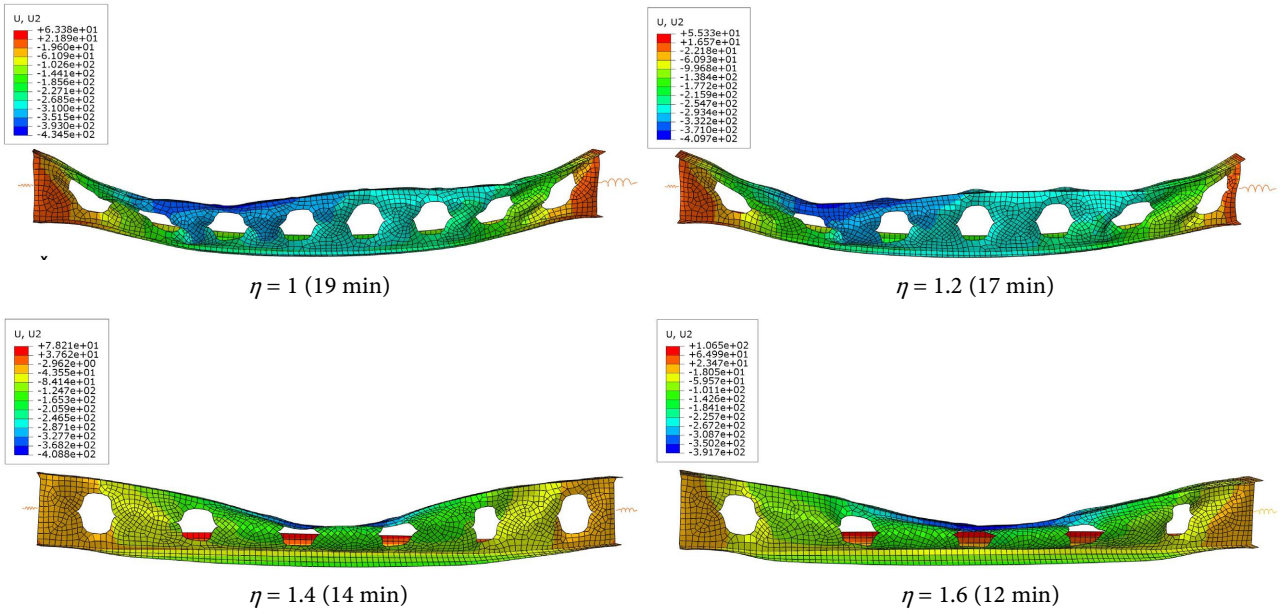

Figure 18. Failure mode of CSBs with varied opening spacing-to-height ratio η.

4.3. Effect of Opening Shape

Nowadays, with the improvement of the cellular beam production industry, the discussion on the shape of the web opening is more and more developed. The opening shapes of the cellular beams studied are rectangular, hexagonal and sinusoidal respectively. The dimension and design parameters of CSBs in this part are as follows: The beam section is H500 × 250 × 12 × 18, span length L = 4.2 m, axial restraint stiffness $\alpha = 1$ and rotational restraint stiffness $\beta = 1$. The 3 groups of beam were loaded by a uniformly distributed load and having simply supported boundary conditions. The opening shape and dimensions of the beam web are described in **Figure 19** and **Table 5**.

The temperature change curves of the axial force and mid-span deflection of the 3 groups of cellular beams are shown in **Figure 20**.

Analyzing the mid-span deflection in **Figure 20(a)**, the deflection development of the cellular beam with rectangular openings is greater than those of the hexagonal and sinusoidal openings. For the hexagonal openings, the mid-span displacement occurs earlier than that of the sinusoidal openings but the difference between the 2 openings is not obvious. In the process of heating, the development trend is basically same, the difference is small. The cellular beam with sinusoidal openings provides a more uniform stress distribution, potentially leading to smoother mid-span displacement curves. Analyzing the axial force shown in **Figure 20(b)**, the axial force of cellular beam with sinusoidal and hexagonal openings methods is basically same at the first stage, but because the edge of the regular hexagonal openings is prone to stress concentration, the plastic effect of the opening angle is more obvious, so it enters elastic-plastic stage earlier. After entering the catenary action stage, the difference in the axial force is not obvious. **Figure 21** presents failure modes and failure time of 3 specimens.

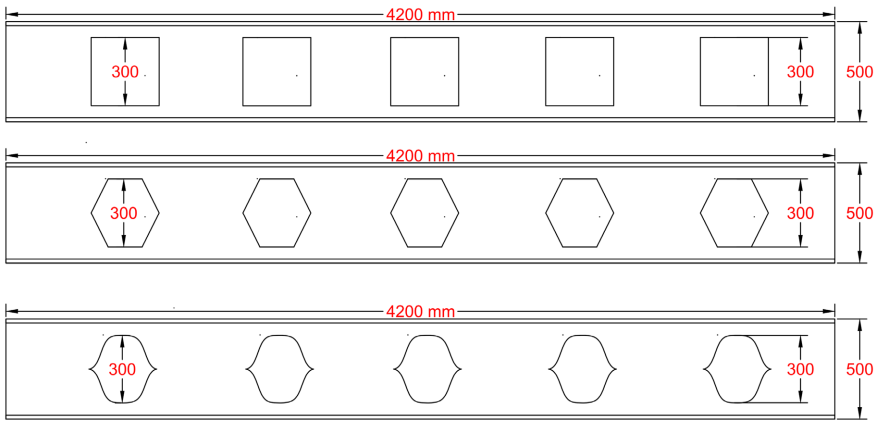

Figure 19. Geometric dimensions of CSBs with different openings shape.

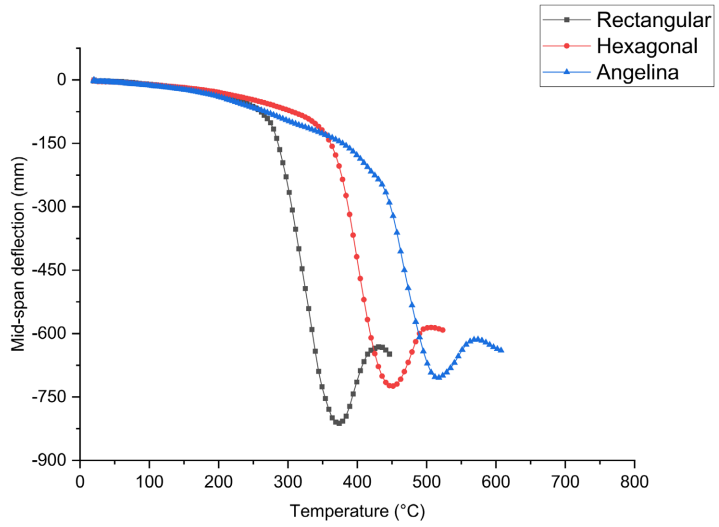

(a)

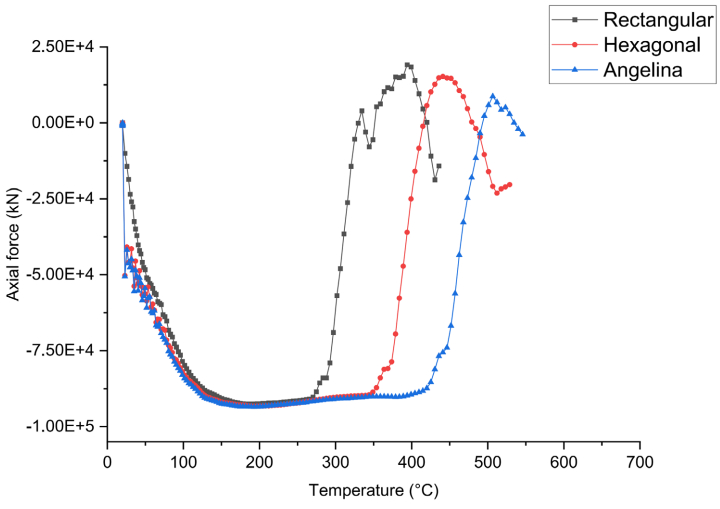

(b)

Figure 20. Effect of openings shape on structural responses of CSBs. (a) Mid-span deflection-temperature curve; (b) Axial force-temperature curve.

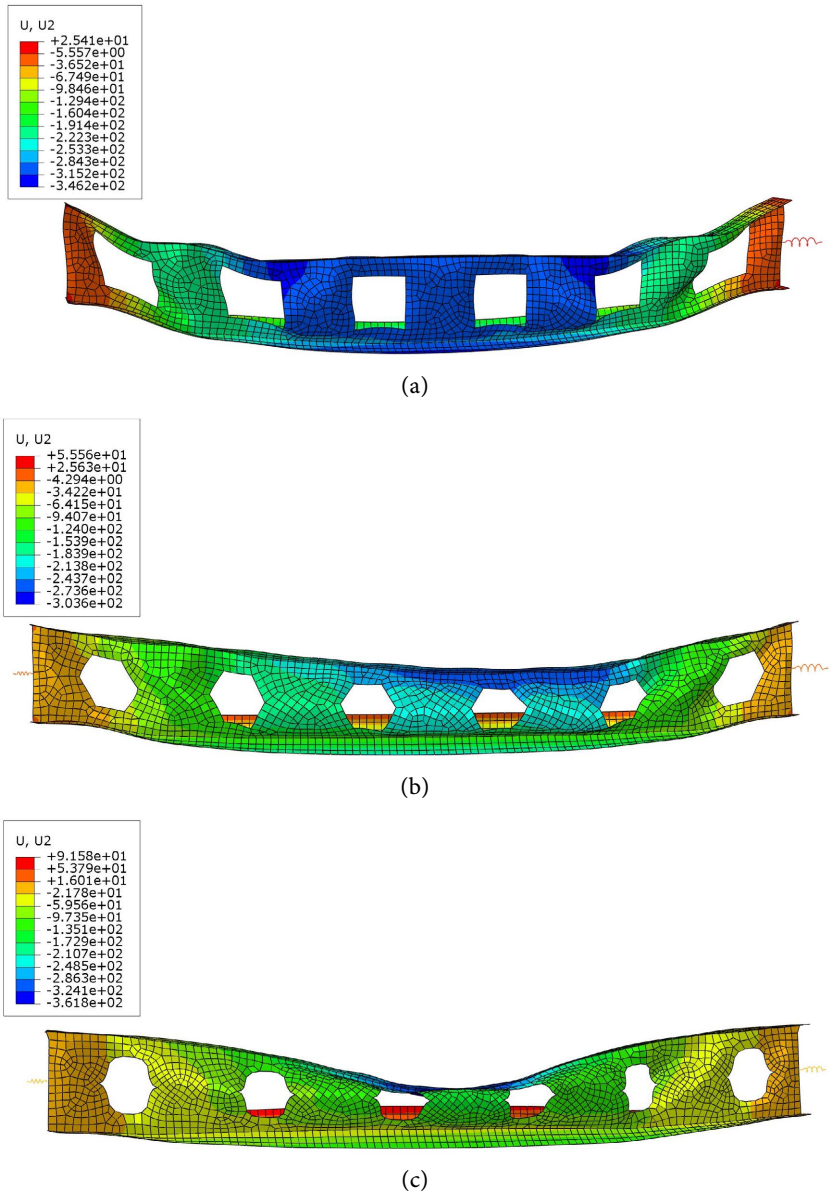

Figure 21. Failure mode of cellular beam with various shapes. (a) Rectangular (14 min), (b) Hexagonal (16 min), (c) Angelina (18 min).

Table 5. Geometric parameters of CSBs with different openings shape.

Opening shape	Rectangular	Hexagonal	Angelina
Opening height (mm)	300	300	300
Opening spacing (mm)	700	700	700
Number of opening holes	6	6	6
Load ratio	0.5	0.5	0.5

The CSBs endure the load and sustain firing for a longer duration compared to the other two specimens.

4.4. Effect of Load Ratio μ

Load ratio μ refers to the ratio of the load-bearing capacity of the CSBs at elevated temperature to its load-bearing capacity at ambient temperature. The load-bearing capacity of CSBs can be varied in different practical conditions; hence μ shall be an essential factor through fire resistance analysis. In design process, the load ratio will not be set too small or too large, considering structural safety and economy. In actual engineering, the common load ratios range from 0.3 to 0.7. In order to comprehensively analyze the influence of load ratios and make the simulation data play a reference role in the design of actual projects, 4 groups of load ratios were selected as 0.4, 0.5, 0.6 and 0.7. The dimension and design parameters of CSBs in this part are as follows: The beam section is H500 × 250 × 12 × 18, span length L = 4.2 m, axial restraint stiffness $\alpha = 1$ and rotational restraint stiffness $\beta = 1$. The beam was loaded by a uniformly distributed load and having simply supported boundary conditions. The geometric parameters of CSBs are shown in Table 6.

The temperature change curves of axial force and mid-span deflection after loading are shown in Figure 22.

According to the analysis of the results, with the increase of the load ratio μ, the changes of the axial force and mid-span deflection are greatly affected, so the load ratio is a vital influencing factor of the structural response of CSBs under fire. It can be seen in Figure 22(a) that the bigger μ is, the sooner mid-span vertical displacement develops, the earlier positive axial deflection produces, and the earlier catenary action occurs. Moreover, catenary action lasts longer since μ grows from 0.6 - 0.7. Comparative analysis of the axial force in Figure 22(b) shows that, the axial force value change significantly: when μ is within 0.4 - 0.6, the difference between the maximum axial force of the three load ratios is large; when $\mu \geq 0.6$, the axial force will decrease rapidly after reaching the maximum axial pressure, which proves that due to the excessive load ratio, the deformation degree of the beam increases obviously, and the axial pressure shortening rate is relatively large.

When the load ratio is within 0.6 - 0.7, the critical temperature T_c is reached prematurely, and the structural safety time is obviously shorter. So under high temperature conditions, the larger μ is, the earlier the mid-span deflection will be, which reflects that the safety time of the structure will decrease with the increase of the load ratio μ. Figure 23 presents failure modes and failure time of 4

Table 6. Geometric parameters of CSBs with different load ratios.

Load ratio μ	0.4	0.5	0.6	0.7
Opening height (mm)	300	300	300	300
Opening spacing (mm)	700	700	700	700
Number of opening holes	6	6	6	6
Fillet radius	75	75	75	75

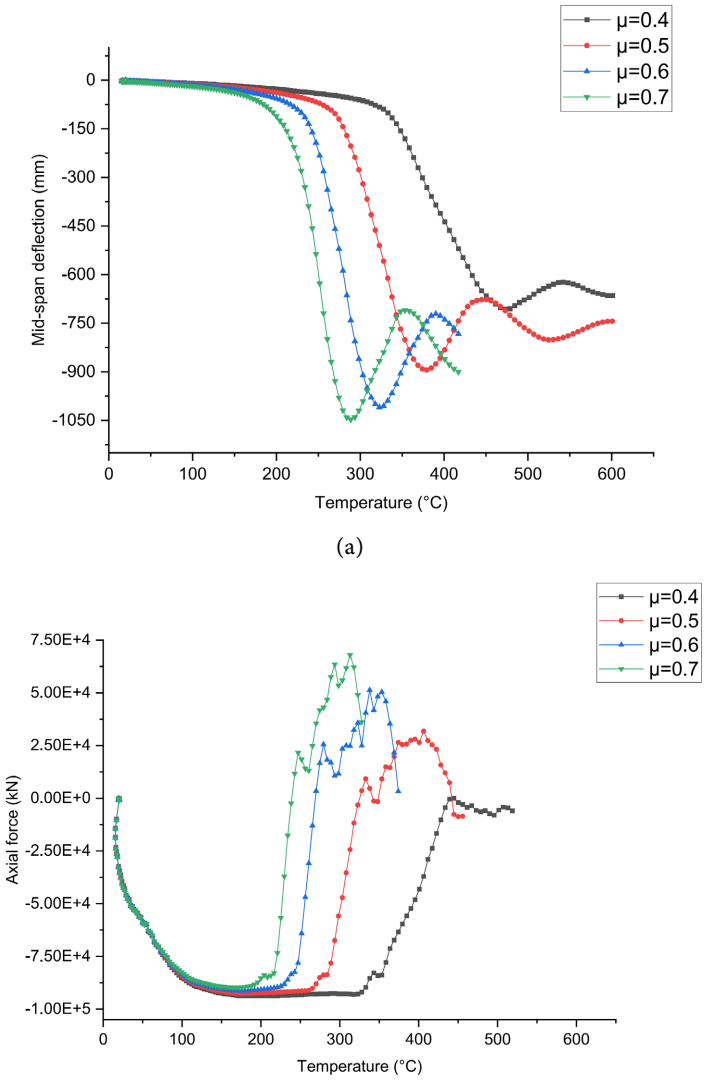

Figure 22. Effect of load ratio μ on structural responses of CSBs. (a) Mid-span deflection-temperature curve; (b) Axial force-temperature curve.

specimens. While μ is less than 0.6, CSBs can undergo the load and fire in a long time. As μ goes to 0.7, the stress of beam web is relatively high, and lower flange yielding at mid-span becomes more obvious. Failure time inclines since more external load applied on the upper flange. The CSBs with μ more than 0.6 can bear the load less than 12 minutes, which is particularly dangerous for public safety when fire occurs. As a conclusion, μ should be maintained within 0.4 - 0.6 to achieve a better fire resistance under high temperatures. Hence, μ can be regarded as one of vital factors while analyzing the fire resistance performance of CSBs.

Table 7 summarize the results of fire resistance perfomance for the cellular steel beams with various parameters under high temperatures rise due to fire using finite element software ABAQUS [18].

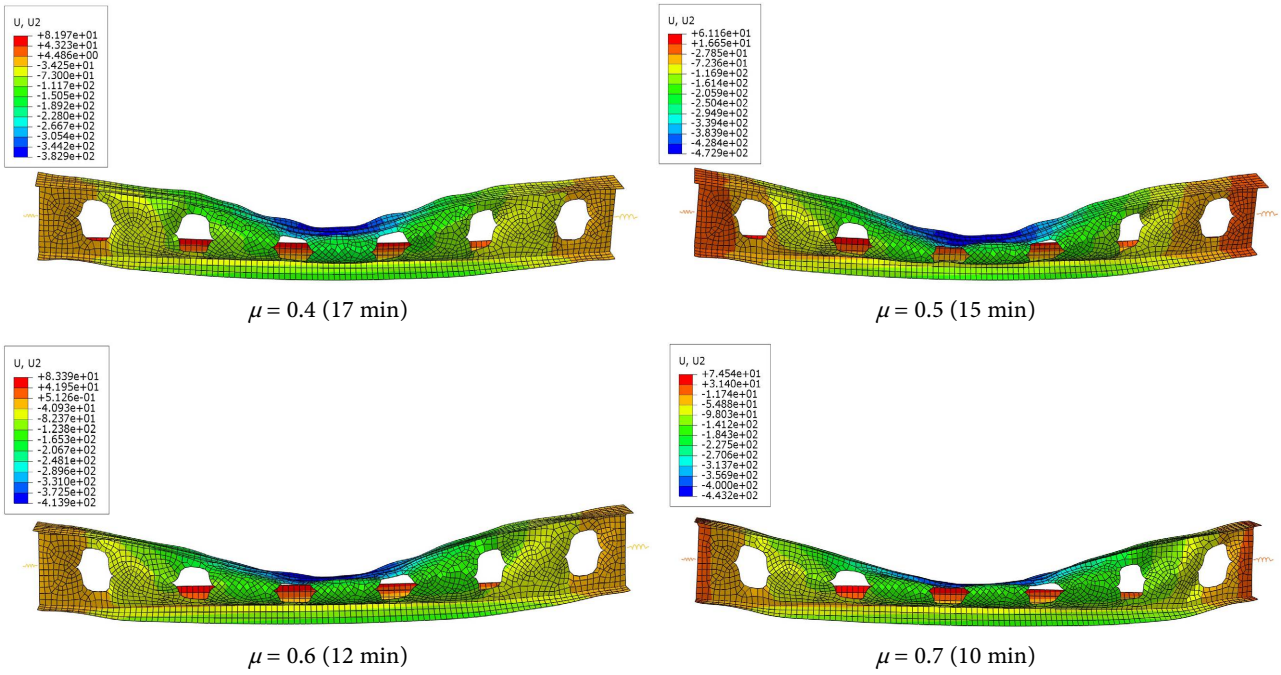

$\mu = 0.4$ (17 min) $\mu = 0.5$ (15 min)

$\mu = 0.6$ (12 min) $\mu = 0.7$ (10 min)

Figure 23. Failure mode of CSBs with varied load ratio μ.

Table 7. Finite element analysis results of cellular steel beams in the parametric study.

Group	Finite element analysis (FEA)					
	Specimen	Max. deflection (mm)	Residual deflection (mm)	Fire resistance (min)	Critical temperature (˚C)	Failure mode
Opening diameter-to-height ratio γ	0.4	−768	−724	18	689	BFB
	0.6	−944	−776	16	574	WB
	0.8	−968	−818	14	404	WB
	0.9	−985	−881	12	344	WB
Opening spacing-to-height ratio η	1	−738	−738	19	724	WB
	1.2	−719	−631	17	707	WB
	1.4	−818	−719	14	467	BFB
	1.6	−907	−742	12	393	BFB
Opening shape	Rectangular	−950	−924	14	446	WB
	Hexagonal	−894	−761	16	467	WB
	Angelina	−663	−580	18	612	BFB
Load ratio μ	0.4	−712	−650	17	623	BFB
	0.5	−887	−754	15	501	BFB
	0.6	−1009	−817	12	390	BFB
	0.7	−1040	−840	10	303	BFB

In Table 7, it can be seen that the cellular steel beams heated using the standard fire curves ISO-834 failed between 18 and 10 min, which is below 30 min fire resistance, depending of various factors during fire. During the heating process, different failure modes were identified from the cellular steel beams in the parametric study. The failure modes comprised of top flange buckling (TFB), bottom flange buckling (BFB), bottom flange yielding (BFY), web buckling (WB), and web yielding (WY).

5. Conclusions

This paper investigates the fire resistance of CSBs with various parameters under high temperatures rise due to fire using finite element software ABAQUS. First, the mechanical parameters of CSBs are analyzed, including load-bearing capacity and the temperature distribution during the heating process. On this basis, through structural analysis simulation of the entire heating process, the structural response of the CSBs is divided into five stages: elastic stage, elastic-plastic stage, self-balancing stage, catenary stage and ultimate destruction stage. Four influencing factors of CSBs beams were analyzed and the following conclusions can be drawn:

1) Among the influencing factors, the opening diameter-to-height ratio γ affects the fire resistance perfomance of CSBs much more than other parameters, with the increase of γ, the axial force and the bearing capacity of CSBs decreases. Therefore, the reasonable interval of opening diameter to-height-ratio is $\gamma \leq 0.8$.

2) Among the influencing factors, opening spacing-to-height ratio η jointly affects the web-post area of the CSBs. Taking into account the steel utilization rate, shear capacity and torsion resistance, the value range of the opening spacing-to-height ratio η is defined as 1 - 1.4. Within a reasonable value range, the deflection basically does not change with changes in spacing-to-height ratio.

3) Among them, the analysis of the web opening shape found that the performance difference between the cellular beam with sinusoidal and hexagonal openings is not obvious. The CSBs has a slight advantage due to its more uniform stress distribution. Cellular beams with sinusoidal openings offer better performance due to its increased area for stress distribution in addition to curved edges that causes smooth stress distribution. The analysis of the remaining influencing factors and the parameter analysis in other part are all based on the cellular beam with sinusoidal openings.

4) The load ratio has a great influence on the fire resistance of CSBs. Considering the fire resistance performance and the deformation of CSBs, the load ratio μ is recommended to be controlled within 0.4 - 0.7.

Acknowledgements

I would like to express my sincere gratitude to my supervisor, Yinghua Yang, for providing me with valuable guidance, support, and encouragement throughout my research. Without his expertise and insights, this work would not have been

possible. Finally, I would like to express my gratitude to my parents, Marcel Sagali and Sidonie Mupanga, for their support and encouragement throughout my academic journey. Their love and encouragement have been a constant source of inspiration for me.

Conflicts of Interest

The authors declare no conflicts of interest regarding the publication of this paper.

References

[1] Chung, K.F. (2002) Composite Beams and Floor Systems Fully Integrated with Building Services. *Progress in Structural Engineering & Materials*, **4**, 169-178. https://doi.org/10.1002/pse.116

[2] Lawson, R.M. (1987) Design for Openings in the Webs of Composite Beams. CIRIA/Steel Construction Institute, CIRIA Special Publication and SCI Publication 068, Ascot.

[3] Chung, K.F., Liu, T.C.H. and Ko, A.C.H., (2001) Investigation on Vierendeel Mechanism in Steel Beams with Circular Web Openings. *Journal of Constructional Steel Research*, **57**, 467-490. https://doi.org/10.1016/S0143-974X(00)00035-3

[4] Liu, T.C.H. and Chung K.F. (2003) Steel Beams with Large Web Openings of Various Shapes and Sizes: Finite Element Investigation. *Journal of Constructional Steel Research*, **59**, 1159-1176. https://doi.org/10.1016/S0143-974X(03)00030-0

[5] Chung, K.F., Liu, T.C.H. and Ko, A.C.H. (2003) Steel Beams with Large Web Openings of Various Shapes and Sizes: An Empirical Design Method Using a Generalised Moment-Shear Interaction Curve. *Journal of Constructional Steel Research*, **59**, 1177-1200. https://doi.org/10.1016/S0143-974X(03)00029-4

[6] Bailey, C. (2004) Indicative Fire Tests to Investigate the Behaviour of Cellular Beams Protected with Intumescent Coatings. *Fire Safety Journal*, **39**, 689-709. https://doi.org/10.1016/j.firesaf.2004.06.007

[7] Bitar, D., Demarco, T. and Martin, P.O. (2005) Steel and Non Composite Cellular Beams—Novel Approach for Design Based on Experimental Studies and Numerical Investigations. EUROSTEEL.

[8] Nadjai, A. (2005) Performance of Cellular Composite Floor Beams at Ambient Temperatures. FireSERT, Test Report.

[9] Nadjai, A., Vassart, O., Ali, F., Talamona, D., Allam, A. and Hawes, M. (2007) Performance of Cellular Composite Floor Beams at Elevated Temperatures. *Fire Safety Journal*, **42**, 489-497. https://doi.org/10.1016/j.firesaf.2007.05.001

[10] Vassart, O., Bailey, C.G., Bihina, G., Hawes, M., Nadjai, A., Peigneux, C., Simms, W.I. and Franssen, J.M. (2010) Parametrical Study on the Behaviour of Steel and Composite Cellular Beams under Fire Conditions. *Proceedings of the Sixth International Conference on Structures in Fire* (*SiF*'10), East Lansing, 2-4 January 2010, 349-357.

[11] Bihina, G., Zhao, B. and Vassart, O. (2009) Cellular Composite Beams at Elevated Temperatures, Experimental Investigation. *Proceedings of International Conference Prague*, Prague, 19-20 April 2013, 537-542.

[12] Vassart, O., Bailey, C.G., Hawes, M., Nadjai, A., Simms, W.I., Zhao, B., Gernay, T. and Franssen, J.M. (2010) Large-Scale Fire Test of Unprotected Cellular Beam Act-

ing in Membrane Action. *Journal of Structural Fire Engineering*, **2**, 259-268. https://doi.org/10.1260/2040-2317.2.4.259

[13] EC3, ENV 1993-1-1 (2005) Eurocode 3: Design of Steel Structures. Part 1-1: General Rules and Rules for Buildings. Annex N. European Committee for Standardization.

[14] Cong, S., Liang, S. and Dong, Y. (2005) Experimental Investigation of Behavior of Simple Supported Steel Beams under Fire. *Journal of Southeast University* (*Natural Science Edition*), **35**, 66-68.

[15] EN 1994-1-2 (2005) Eurocode 4: Design of Composite Steel and Concrete Structures. Part 1-2: General rules. Structural Fire Design. European Committee for Standardization (CEN).

[16] EN 1991-1-2 (2003) Eurocode 1: Actions on Structures. Part 1-2: General Actions. Actions on Structures Exposed to Fire. European Committee for Standardization (CEN).

[17] EN 1993-1-2 (2005) Eurocode 3: Design of Steel Structures. Part 1-2: General Rules. Structural Fire Design. European Committee for Standardization (CEN)

[18] ABAQUS/Standard Version 6.12, Dassault Systèmes, Providence, RI, USA.